Fast modal reconstruction of large plane wavefronts from sparse measurements using Shack-Hartmann sensors

NIKOLAUS BERLAKOVICH[1*], ERNST CSENCSICS[1], DAMIAN SENONER[1], AND GEORG SCHITTER[1]

[1] *Automation and Control Institute (ACIN), TU Wien, 1040 Vienna, Austria*
[*] *Corresponding author: berlakovich@acin.tuwien.ac.at*

Compiled April 12, 2023

A concept for the fast measurement and reconstruction of optical wavefronts using Shack-Hartmann sensors (SHS) is presented. For wavefronts with a diameter at the scale of several tens of millimeters, hundreds of measurements with an SHS may be necessary to cover the wavefront. In the proposed concept a few SHS are used to measure about 2 % of the entire wavefront, providing sufficient measurement data for a successful reconstruction of the wavefront. The small number of SHS mounted in parallel makes the concept suitable for time-critical applications. A simulation analysis is performed and an experimental validation of the concept is presented, demonstrating that the wavefront can be reconstructed with an RMS error of about 100 nm.

OCIS codes: (150.1135) Algorithms; (120.3940) Metrology; (120.5050) Phase measurement; (220.4840) Testing; (280.4788) Optical sensing and sensors.

http://dx.doi.org/10.1364/ao.XX.XXXXXX

1. INTRODUCTION

Wavefront sensors are frequently used in industry for assessing optical systems. By measuring the optical wavefront, they provide non-contact measurements of optical systems and enable a direct measurement of the optical performance. Especially, Shack-Hartmann sensors (SHS) are popular wavefront sensors, because of their compactness, insensitivity to vibrations, and reference-free measurement [1, 2]. To enable the measurement of wavefronts with a diameter larger than the diameter of the sensor aperture shrinking optics in combination with null optics can be used. However, supporting optics can reduce the accuracy of the measurement, as they may cause additional errors in the wavefront [3]. In an alternative approach, the wavefront is scanned with an SHS, such that no supporting optics are necessary [4–6]. Using a positioning system, the SHS measures the wavefront at several locations. The measurements partially overlap to enable the reconstruction of the wavefront using registration algorithms [7–11]. While the registration can be carried out in hundreds of milliseconds, the measurement can be time-consuming, as a large number of SHS measurements (>100) are necessary to cover the entire wavefront. This may result in measurement times of minutes unsuitable for time-critical applications, such as inline metrology.

The contribution of this paper is a concept for the sparse measurement and modal reconstruction of large plane wavefronts using SHS. This enables a significant decrease in the measurement time as compared to a registration-based approach. Section 2 introduces the concept. Section 3 presents a simulation analysis of the concept and Section 4 presents an experimental proof of the concept. Section 5 concludes the paper.

2. CONCEPT

A. Wavefront measurement

The wavefront is measured with an SHS at a few positions as illustrated in Fig. 1a. A percentage of about 2% of the wavefront is measured and used to reconstruct the wavefront.
The SHS measures the gradients of the wavefront at grid points defined by the lenslet array in the aperture of the sensor. This results in a set of gradient measurements for each sensor position. The sets of gradient measurements and the respective sensor positions are then used to estimate the wavefront. In particular, the coefficients of a linear combination of polynomials, e.g. Zernike polynomials [12], are estimated from the measurement data where the linear combination corresponds to the estimated

wavefront.
In Fig. 1b an experimental setup is illustrated. In front of the measurement system, a condenser lens is positioned generating a wavefront with a diameter of around 92 mm. The measurement system consists of 5 SHS which measure in total 1.4% of the wavefront. In Section 4 details with respect to the setup are presented and an experimental evaluation of the concept is discussed.

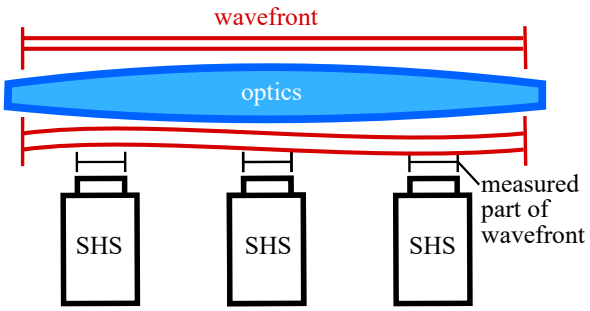

(a)

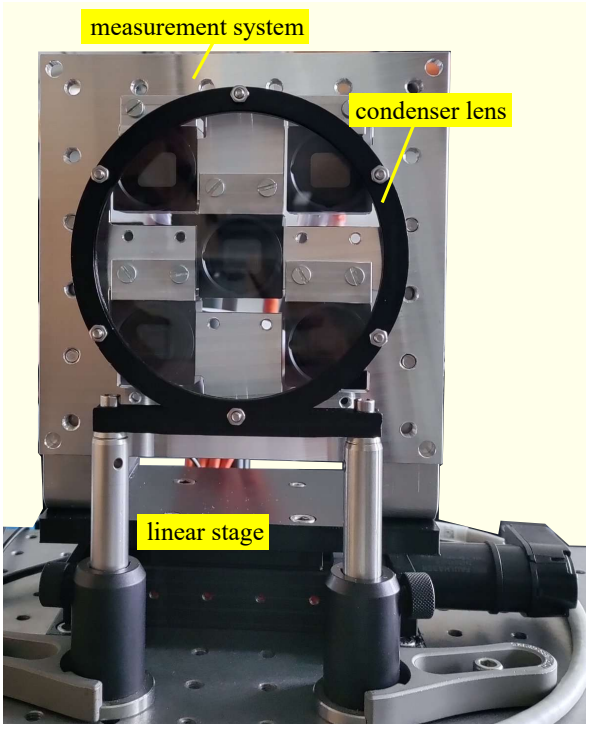

(b)

Fig. 1. (a) Measurement concept. The wavefront is measured at a few positions with an SHS. (b) Experimental setup of the measurement concept. The measurement system comprises 5 SHS. A condenser lens generates a plane wavefront which is measured by the system.

B. Wavefront reconstruction

The nominal positions of the gradient measurements in the global frame (FG) are given by

$$\mathbf{x}_{ul} = \mathbf{r}_u + \mathbf{x}_l \quad \text{with} \quad \mathbf{x}_{ul} = (x_{1ul}, x_{2ul}) \in \mathbb{R}^2, \tag{1}$$

where $\mathbf{r}_u$ is the nominal position of SHS u ($u = 1..U$) and $\mathbf{x}_l$ is the position of the lenslet l ($l = 1..L$) in the local coordinate system of the SHS, as illustrated in Fig. 2. For a position $\mathbf{x}_{ul}$, the

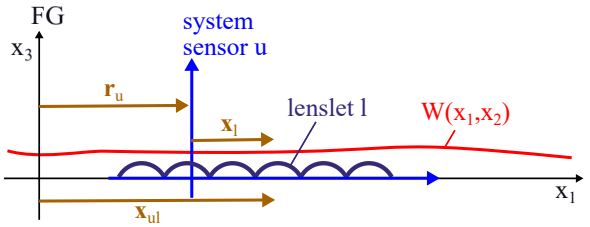

Fig. 2. $\mathbf{x}_{ul}$ is the nominal position of one gradient measurement (one lenslet) in FG.

measured gradient is represented by two scalar values, i.e.

$$g_{ulk} = \frac{dW}{dx_k}\Big|_{\mathbf{x}_{ul}} + \varepsilon_{ulk} \quad \text{with} \quad k = 1, 2 \quad , \tag{2}$$

where W denotes the wavefront and ε_{ulk} the measurement error. To enable the modal reconstruction of the wavefront, it is assumed that the wavefront is well described by a linear combination of polynomials.

$$W = \sum_{n=1}^{N} c_n Z_n, \tag{3}$$

where Z_n denotes a polynomial and $c_n \in \mathbb{R}$ the respective unknown coefficient. In this paper, Zernike polynomials are used in Eq. 3. The coefficients are estimated in the least squares sense [13], where a quadratic optimization problem given by

$$\begin{aligned} &\min_{c_1..c_N} \sum_{u,l,k} \left(g_{ulk} - \frac{dW}{dx_k}\Big|_{\mathbf{x}_{ul}}\right)^2 \\ &= \min_{c_1..c_N} \sum_{u,l,k} \left(g_{ulk} - \sum_n c_n \frac{dZ_n}{dx_k}\Big|_{\mathbf{x}_{ul}}\right)^2, \end{aligned} \tag{4}$$

is solved. To avoid coupling effects all polynomials with a non-zero coefficient have to be considered in Eq. 3 [14].
The measurement error (ε_{ulk}) is caused by noise as well as misalignment of the sensor, i.e. a deviation of the sensor from its nominal position and alignment. Translational misalignment defines the deviation from the nominal position and is described by three parameters, each corresponding to a translation of the sensor with respect to one spatial dimension. Rotational misalignment corresponds to a deviation from the nominal alignment and is defined by three angles reflecting roll, pitch, and yaw of the sensor (see Fig. 3). Simulation analysis shows that the estimation of the coefficients is highly sensitive to pitch and yaw and a reduction of the influence of these quantities on the estimation is typically necessary. The contributions of pitch and yaw to the measurement error (ε_{ulk}) at position $\mathbf{x}_{ul}$ can be expressed by

$$\begin{aligned} \varepsilon_{ul1} &= \varepsilon_{ul1}^{rest} + \eta_u^{yaw} \quad \text{and} \\ \varepsilon_{ul2} &= \varepsilon_{ul2}^{rest} + \eta_u^{pitch}, \end{aligned} \tag{5}$$

Post-print version of the article: Nikolaus Berlakovich, Ernst Csencsics, Damian Senoner, and Georg Schitter , "Fast modal reconstruction of large plane wavefronts from sparse measurements using Shack–Hartmann sensors," *Applied Optics*, Vol. 62, Issue 26, pp. 6986-6992, 2023. DOI: 10.1364/AO.493076

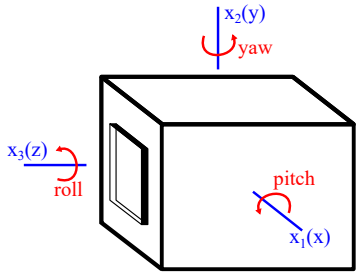

Fig. 3. Rotational misalignment of the SHS.

where ε_{ulk}^{rest} comprises the contributions of all other error sources. Pitch and yaw have no influence on the derivative of the wavefront with respect to x_1 and x_2, respectively, which enables the following compact expression of Eq. 5

$$\varepsilon_{ulk} = \varepsilon_{ulk}^{rest} + \eta_{uk} \quad \text{with} \quad k = 1,2, \tag{6}$$

where η_{uk} is the measurement error caused by pitch and yaw. The fact that η_{uk} does not depend on the lenslet index l, motivates the additional estimation of this error to obtain a decoupling of the coefficients and pitch and yaw. For this, Eq. 4 is extended to the following optimization problem

$$\min_{c_1..c_N,\eta_{11}..\eta_{U2}} \sum_{u,l,k} \left(g_{ulk} - \eta_{uk} - \sum_n c_n \frac{dZ_n}{dx_k}\Big|_{\mathbf{x}_{ul}}\right)^2, \tag{7}$$

which corresponds to the least squares estimation of the coefficients and the error caused by pitch and yaw. Owing to the decoupling, a significant reduction of the influence of pitch and yaw on the estimation of the coefficients is obtained. If the Zernike polynomials for vertical and horizontal tilt are used in Eq. 3, two terms are added to Eq. 7 given by

$$\left(\sum_u \eta_{u1}\right)^2 \quad \text{and} \quad \left(\sum_u \eta_{u2}\right)^2. \tag{8}$$

With these terms, the mean values of the pitch and yaw of the sensors are defined as 0. Owing to this definition unique results for the coefficients of vertical and horizontal tilt are obtained. The problem of Eq. 7 can be transformed to a matrix equation given by

$$\boldsymbol{Q}^T \boldsymbol{Q}\, \boldsymbol{A} = \boldsymbol{Q}^T \boldsymbol{G}, \tag{9}$$

with $\boldsymbol{Q} \in \mathbb{R}^{(2UL)\times(N+2U)}$, $\boldsymbol{A} \in \mathbb{R}^{N+2U}$ and $\boldsymbol{G} \in \mathbb{R}^{2UL}$. The explicit expressions of the quantities of Eq. 9 are as follows:

$$\boldsymbol{Q} = \begin{pmatrix} \frac{dZ_1}{dx_1}\Big|_{\mathbf{x}_{11}} & .. & \frac{dZ_N}{dx_1}\Big|_{\mathbf{x}_{11}} & 1 & 0 & 0 & .. & 0 \\ \frac{dZ_1}{dx_2}\Big|_{\mathbf{x}_{11}} & .. & \frac{dZ_N}{dx_2}\Big|_{\mathbf{x}_{11}} & 0 & 1 & 0 & .. & 0 \\ \vdots & & \vdots & & & \vdots & & \vdots \\ \frac{dZ_1}{dx_1}\Big|_{\mathbf{x}_{UL}} & .. & \frac{dZ_N}{dx_1}\Big|_{\mathbf{x}_{UL}} & 0 & .. & 0 & 1 & 0 \\ \frac{dZ_1}{dx_2}\Big|_{\mathbf{x}_{UL}} & .. & \frac{dZ_N}{dx_2}\Big|_{\mathbf{x}_{UL}} & 0 & .. & 0 & 0 & 1 \end{pmatrix}, \tag{10}$$

$$\boldsymbol{A} = \begin{pmatrix} c_1 \\ \vdots \\ c_N \\ \eta_{11} \\ \eta_{12} \\ \vdots \\ \eta_{U1} \\ \eta_{U2} \end{pmatrix} \quad \text{and} \quad \boldsymbol{G} = \begin{pmatrix} g_{111} \\ g_{112} \\ \vdots \\ \vdots \\ \vdots \\ \vdots \\ g_{UL1} \\ g_{UL2} \end{pmatrix}. \tag{11}$$

The additional estimation of the misalignment parameters, suggested by Eq. 7, is successful as long as $\boldsymbol{Q}$ remains well-conditioned, meaning that the column vectors in $\boldsymbol{Q}$ are not too close to linear dependence. This is important to keep the influence of measurement errors, such as noise, sufficiently small. If the column vectors are too close to linear dependence, Eq. 7 does not lead to the desired decoupling and additional measurements have to be carried out to calibrate the system with respect to the misalignment parameters.

3. SIMULATION ANALYSIS

In the following sections, the dependence of the reconstruction performance on the number of sensors, sensor misalignment, and measurement noise is analyzed. In particular, the influence of one quantity on the reconstruction error is evaluated per section, while the other quantities remain equal to a reference configuration introduced in Section A.

A. Simulation settings

The simulated wavefront consists of a combination of the first 15 Zernike polynomials and is illustrated in Fig. 4. It has a peak-to-valley (PV) of 14 μm and a diameter of 92 mm. The measurement with an SHS is simulated using in-house software based on Matlab (The MathWorks Inc., Natick, MA, USA) and OpticStudio (Zemax LLC, Kirkland, WA, USA). Measurement noise as well as sensor misalignment are simulated to obtain a realistic simulation. With the simulated measurement data, the wavefront is reconstructed based on the algorithm presented in Section B. In particular, the estimator of Eq. 7 is used to determine the coefficients of the Zernike polynomials of the first 4 orders, leading to 14 coefficients as piston cannot be determined from gradient measurements.

To evaluate the result, the reconstruction error is determined, which is defined as the difference between the exact wavefront and the reconstructed wavefront. Before the difference between the wavefronts is determined, the reconstructed wavefront is fitted into the exact wavefront using rigid body transformation and wavefront propagation to compensate for misalignment and phase differences between the wavefronts [7].

A simulation with 5 SHS is presented in this section where the respective simulation settings are used as a reference configuration in the simulation analysis of the subsequent sections. The nominal sensor positions are given by

$$(x,y)\,[mm] = (0,0),\ (30,30),\ (30,-30),\ (-30,30),\ (-30,-30),$$

and are illustrated in Fig. 5a, where the red squares represent the sensor apertures with a side length of 3.9 mm. Each sensor aperture includes a 52×52 lenslet array (2704 lenslets) with each

Post-print version of the article: Nikolaus Berlakovich, Ernst Csencsics, Damian Senoner, and Georg Schitter , "Fast modal reconstruction of large plane wavefronts from sparse measurements using Shack–Hartmann sensors," *Applied Optics*, Vol. 62, Issue 26, pp. 6986-6992, 2023. DOI: 10.1364/AO.493076

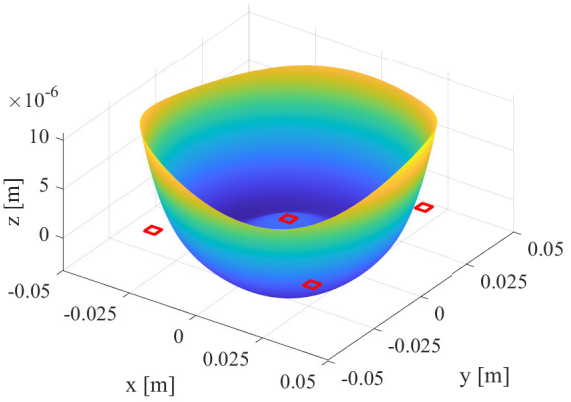

Fig. 4. The wavefront (PV=14 μm) is a linear combination of the first 15 Zernike polynomials and measured at 5 sensor positions (sensor apertures illustrated with red squares).

lenslet covering an area of $75 \times 75\,\mu m^2$. Noise in the gradient measurements is simulated with a standard deviation of the angle of slope equal to 30 μrad, which is a realistic value for noise in an SHS [15]. All sensors are randomly misaligned, where the translational and rotational misalignment have an expected standard deviation of 100 μm and 1 $mrad$, respectively [16]. With five SHS 1.4 % of the wavefront is measured. The wavefront is reconstructed with the measurement data and the respective reconstruction error is shown in Fig. 5b. The RMS value of the reconstruction error is equal to 99 nm. The wavefront is successfully reconstructed using the estimator of Eq. 7, where the pitch and yaw of the sensors are estimated along with the Zernike-coefficients. Simulation shows that the pitch and yaw of each sensor are estimated with a relative error of around 2 %.

B. Influence of sensor number

Sensor configurations with 3, 5, 13, and 17 SHS are considered for the evaluation of the number of sensors. As the reconstruction of the wavefront is influenced by the sensor arrangement as well, lower-number sensor configurations are included in higher-number sensor configurations, leading to a better observation of the effects related to the number of sensors. The arrangement of the sensors for all configurations is illustrated in Fig. 6a. The dependence of the RMS reconstruction error on the number of SHS is illustrated in Fig. 6b. As expected, the reconstruction error decreases with a higher number of sensors, as with more measurements the influence of noise and sensor misalignment on the estimation of the coefficients (see Eq. 6) decreases. For sensor numbers below 5, the reconstruction error appears highly sensitive to the number of sensors, resulting in a decrease of the RMS reconstruction error by a factor of 24 when increasing the number of sensors from 3 to 5. A further increase to 17 sensors measuring 4.6 % of the wavefront leads to a decrease of the RMS reconstruction error from 99 nm (5 sensors) to 25 nm.

C. Influence of sensor misalignment

Uncertainties in manufacturing and assembly lead to a misalignment of the lenslet array within the housing of the sensor and a misalignment of the sensors mounted in the experimental setup

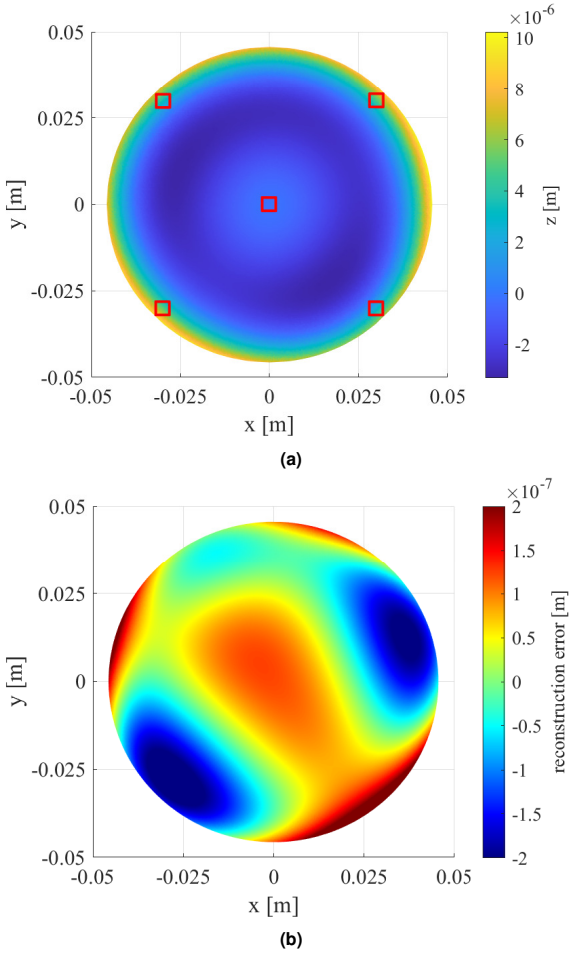

Fig. 5. (a) Arrangement of the 5 SHS (red squares illustrate sensor apertures). (b) Difference between the reconstructed wavefront and the exact wavefront (=reconstruction error) with an RMS value of 99 nm.

(see Fig. 1b). The combination of the misalignment of the lenslet array and the sensor can be considered as a misalignment of the ideal sensor in the experimental setup, where in the ideal sensor no misalignment of the lenslet array exists. The misalignment is divided into translational and rotational misalignment, where each type of misalignment is described by three parameters (see Section B). In the simulation, values drawn from a zero-mean Gaussian distribution are assigned to the parameters of misalignment. The dependence of the RMS reconstruction error on the standard deviation (σ) of the translational misalignment of the ideal sensor is depicted in Fig. 7. Two curves are determined, each for a specific σ of rotational misalignment (i.e., pitch, yaw and roll) equal to 1 and 2 $mrad$. An approximately linear dependence of the reconstruction error on the translational misalignment is observed, where the RMS reconstruction error increases by about 1.4 nm if σ of the translational misalignment is increased by 10 μm. An increase of σ of rotational misalignment from 1 to 2 $mrad$ results in an increase of the RMS reconstruction error of about 2 nm.

Post-print version of the article: Nikolaus Berlakovich, Ernst Csencsics, Damian Senoner, and Georg Schitter , "Fast modal reconstruction of large plane wavefronts from sparse measurements using Shack–Hartmann sensors," *Applied Optics*, Vol. 62, Issue 26, pp. 6986-6992, 2023. DOI: 10.1364/AO.493076

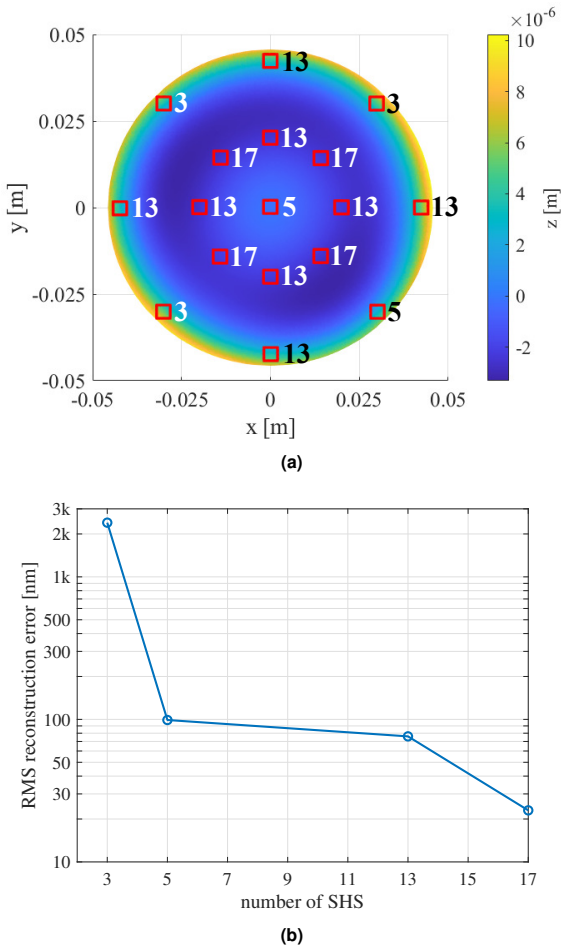

Fig. 6. (a) Arrangement of the SHS. A sensor aperture (=red square) is used for each number of sensors greater or equal to the value next to the aperture. (b) Dependence of the RMS reconstruction error (logarithmic scale) on the number of SHS.

D. Influence of noise

There are different sources for measurement noise, such as background light, readout, or dark currents [17]. The gradient measurement at a lenslet provides two values corresponding to the slopes of the wavefront with respect to the two spatial dimensions in the plane of the lenslet array. The noise is simulated by adding an individual error to each measured slope where the error is drawn from a Gaussian distribution with a mean of zero. The dependence of the RMS reconstruction error on the standard deviation of the noise is illustrated in Fig. 8. A linear relationship between the two quantities is observed where the RMS reconstruction error starts at 23 nm ($\sigma = 0\,\mu rad$) and increases by around 27 nm if σ is increased by 10 μrad. For $\sigma = 60\,\mu rad$ the RMS reconstruction error is 185 nm.

4. EXPERIMENTAL VALIDATION OF THE CONCEPT

The experimental setup is illustrated in Fig. 1b. The measurement system consists of 5 commercial SHS (AR3, Optocraft,

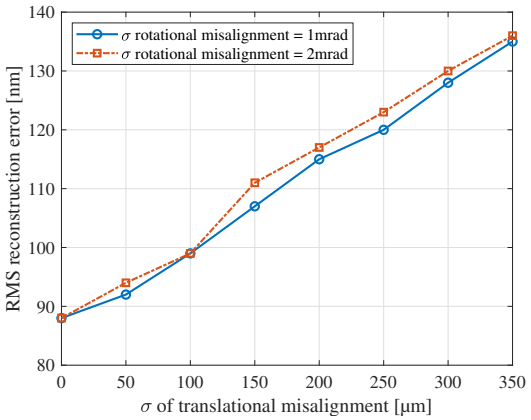

Fig. 7. Dependence of the RMS reconstruction error on σ of translational misalignment of the SHS. The two curves are each with respect to a specific rotational misalignment with σ equal to 1 and 2 $mrad$.

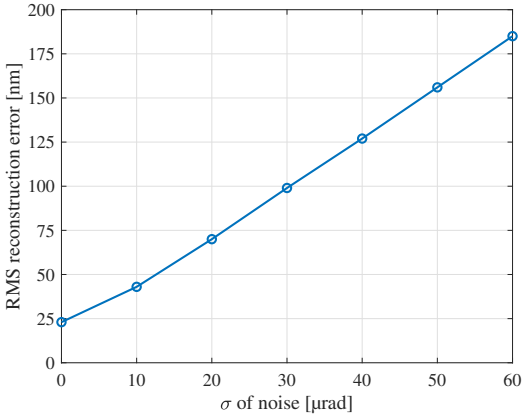

Fig. 8. Dependence of the RMS reconstruction error on σ of the noise in the measurement.

Post-print version of the article: Nikolaus Berlakovich, Ernst Csencsics, Damian Senoner, and Georg Schitter , "Fast modal reconstruction of large plane wavefronts from sparse measurements using Shack–Hartmann sensors," *Applied Optics*, Vol. 62, Issue 26, pp. 6986-6992, 2023. DOI: 10.1364/AO.493076

Erlangen, Germany) with an arrangement equal to Fig. 5a. The lenslet array of one SHS contains 65 × 49 lenslets (3185 in total) with a lens-pitch of 75 × 75 μm^2 resulting in a detection area of 4.9 × 3.7 mm^2. The sensors are mounted on an aluminum frame. A condenser lens with a diameter of 100 mm and a focal length of 400 mm is positioned in front of the measurement system converting a spherical wavefront, generated by a multi-mode fiber, into a plane wavefront, which is then measured by the system. The 5 SHS measure in total 1.4 % of the entire wavefront. The housing of the SHS with a cross-section of 29 × 29 mm^2 limits the number of sensors per unit area. In Eq. 3 the Zernike polynomials of the first 4 orders are considered to describe the wavefront.

After the reconstruction of the entire wavefront with a diameter of 92 mm, the measurement system is laterally shifted by ±10 mm to enable the measurement of the wavefront at different locations. A linear stage is used for shifting the measurement system (see Fig. 1b). In total, the wavefront is measured at 6 distinct locations that are not used to reconstruct the wavefront. For each location, the measured wavefront segment is reconstructed using a state-of-the-art reconstruction algorithm [18]. Owing to the high density of the gradient measurements, the segments are precisely reconstructed with an RMS reconstruction error of a few nanometers. The 6 segments are then fitted into the entirely reconstructed wavefront at the respective measurement locations and the RMS difference between the segments and the wavefront is determined as a measure of the reconstruction quality.

The wavefront is reconstructed one time with the estimator of Eq. 4 (pitch/yaw-estimation off) and one time with the estimator of Eq. 7 (pitch/yaw-estimation on) and the results are illustrated in Fig. 9a and Fig. 9b, respectively. The fitted segments are also depicted. The estimator of Eq. 7, successfully reconstructs the wavefront, as it attains a small RMS difference between the segments and the wavefront of 9.5 nm. Using the estimator of Eq. 4, where pitch and yaw are not estimated, leads to an RMS difference of 112 nm. The result shows the high sensitivity of the estimation quality with respect to pitch and yaw, underlining the importance of the calibration of the system with respect to these misalignment parameters, as suggested by Eq. 7.

The measurement time of one SHS is at the scale of 40 ms and the data is sent to a personal computer (2.6 GHz) where the reconstruction of the wavefront is carried out in about 60 ms.

In summary, the reconstruction of a large plane optical wavefront (diameter = 92 mm) from a sparse measurement covering about 2 % of the wavefront is successfully demonstrated. A few SHS are used for the measurement. The wavefront is reconstructed with an RMS error at the scale of 100 nm suitable for the evaluation of optical systems.

5. CONCLUSIONS

The paper proposes a concept for the sparse measurement and modal reconstruction of large plane wavefronts. A small fraction of the wavefront is measured with a few SHS, and least squares estimation is used to reconstruct the wavefront from the measurements. A simulation analysis is carried out to evaluate the reconstruction quality as well as the influence of measurement errors, such as noise and misalignment of the sensors. Analysis shows that a wavefront with a diameter of 92 mm can be reconstructed with an RMS error of about 100 nm after a measurement of 2 % of the wavefront. Furthermore, the functionality of the concept is experimentally proven with a measurement system containing 5 SHS. As the concept enables low measurement times, it is suitable for time-critical applications including the assessment of optical systems that generate large wavefronts with a diameter of several tens of millimeters.

The relation between the reconstruction performance and the positions of the sensors is part of future research revealing sensor arrangements optimized for the estimation of specific Zernike modes in the wavefront.

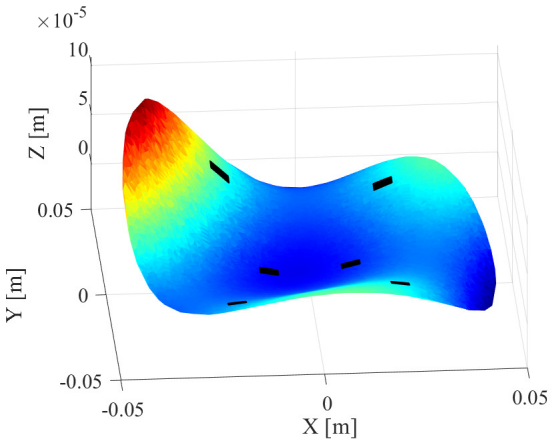

(a) pitch/yaw-estimation off
RMS difference = 112 nm

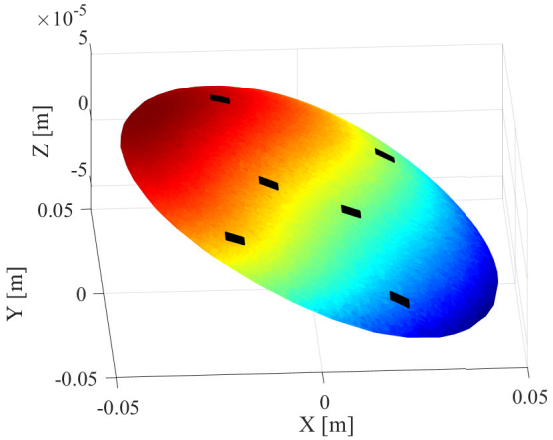

(b) pitch/yaw-estimation on
RMS difference = 9.5 nm

Fig. 9. Six additional segments (black rectangles) of the wavefront are measured and fitted into the reconstructed wavefront. The RMS difference between the segments and the wavefront is a measure of the reconstruction performance, as the segments are not used for the reconstruction.

Acknowledgement. We thank Ulrich Berg from Optocraft GmbH for his support and fruitful discussions.

Disclosures. The authors declare no conflicts of interest.

Data availability. Data underlying the results presented in this paper are not publicly available at this time but may be obtained from the authors upon reasonable request.

Post-print version of the article: Nikolaus Berlakovich, Ernst Csencsics, Damian Senoner, and Georg Schitter , "Fast modal reconstruction of large plane wavefronts from sparse measurements using Shack–Hartmann sensors," *Applied Optics*, Vol. 62, Issue 26, pp. 6986-6992, 2023. DOI: 10.1364/AO.493076

REFERENCES

1. R. K. Tyson, *Adaptive optics engineering handbook* (Marcel Dekker New York, 2000).
2. J. Sheldakova, A. Kudryashov, V. Zavalova, and P. Romanov, "Shack-hartmann wavefront sensor versus fizeau interferometer for laser beam measurements," in *Laser Resonators and Beam Control XI,* vol. 7194 (International Society for Optics and Photonics, 2009), p. 71940B.
3. M. Rocktäschel and H. Tiziani, "Limitations of the shack–hartmann sensor for testing optical aspherics," Opt. & Laser Technol. **34**, 631–637 (2002).
4. D. R. Burada, K. K. Pant, M. Bichra, G. S. Khan, S. Sinzinger, and C. Shakher, "Experimental investigations on characterization of freeform wavefront using shack–hartmann sensor," Opt. Eng. **56**, 084107 (2017).
5. M. E. Fuerst and G. Schitter, "Scanning wavefront sensor for measurement of highly divergent wavefronts," IFAC-PapersOnLine. **52**, 25–30 (2019).
6. M. E. Fuerst, E. Csencsics, N. Berlakovich, and G. Schitter, "Automated measurement of highly divergent optical wavefronts with a scanning shack–hartmann sensor," IEEE Transactions on Instrumentation Meas. **70**, 1–9 (2020).
7. N. Berlakovich, M. E. Fuerst, E. Csencsics, and G. Schitter, "Robust wavefront segment registration based on a parallel approach," Appl. Opt. **60**, 1578–1586 (2021).
8. N. Berlakovich, E. Csencsics, M. Fuerst, and G. Schitter, "Fast, precise, and shape-flexible registration of wavefronts," Appl. Opt. **60**, 6781–6790 (2021).
9. N. Berlakovich, E. Csencsics, M. Fuerst, and G. Schitter, "Iterative parallel registration of strongly misaligned wavefront segments," Opt. Express **29**, 33281–33296 (2021).
10. N. Berlakovich, M. Fuerst, E. Csencsics, and G. Schitter, "Improving the precision of parallel registration by incorporating a priori information," Opt. Express **30**, 41473–41491 (2022).
11. S. Chen, S. Li, and Y. Dai, "Iterative algorithm for subaperture stitching interferometry for general surfaces," JOSA A **22**, 1929–1936 (2005).
12. V. Lakshminarayanan and A. Fleck, "Zernike polynomials: a guide," J. Mod. Opt. **58**, 545–561 (2011).
13. S. J. Miller, "The method of least squares," Math. Dep. Brown Univ. **8**, 1–7 (2006).
14. J. Herrmann, "Cross coupling and aliasing in modal wave-front estimation," JOSA. **71**, 989–992 (1981).
15. D. R. Neal, J. Copland, and D. A. Neal, "Shack-hartmann wavefront sensor precision and accuracy," in *Advanced Characterization Techniques for Optical, Semiconductor, and Data Storage Components,* vol. 4779 (International Society for Optics and Photonics, 2002), pp. 148–160.
16. J. Ma, D. Lu, and W. Zhao, "Assembly errors analysis of linear axis of cnc machine tool considering component deformation," The Int. J. Adv. Manuf. Technol. **86**, 281–289 (2016).
17. H. Mao, Y. Liang, J. Liu, and Z. Huang, "A noise error estimation method for shack-hartmann wavefront sensor," in *AOPC 2015: Telescope and Space Optical Instrumentation,* vol. 9678 (International Society for Optics and Photonics, 2015), p. 967811.
18. L. Huang, J. Xue, B. Gao, C. Zuo, and M. Idir, "Spline based least squares integration for two-dimensional shape or wavefront reconstruction," Opt. Lasers Eng. **91**, 221–226 (2017).

Post-print version of the article: Nikolaus Berlakovich, Ernst Csencsics, Damian Senoner, and Georg Schitter , "Fast modal reconstruction of large plane wavefronts from sparse measurements using Shack–Hartmann sensors," *Applied Optics*, Vol. 62, Issue 26, pp. 6986-6992, 2023. DOI: 10.1364/AO.493076